Understanding the Bifurcation Structure of Robust Chaos in Piecewise-Linear Maps using Renormalisation

Indranil Ghosh, Robert I. McLachlan, David J. W. Simpson

School of Mathematical and Computational Sciences
Massey University, Palmerston North, New Zealand

July 17, 2023

Border-collision normal form

- Piecewise-linear maps arise when modeling systems with switches, thresholds and other abrupt events.
- In our project, we study the two-dimensional *border-collision normal form* (Nusse & Yorke, 1992), given by

$$f_\xi(x,y) = \begin{cases} \begin{bmatrix} \tau_L & 1 \\ -\delta_L & 0 \end{bmatrix} \begin{bmatrix} x \\ y \end{bmatrix} + \begin{bmatrix} 1 \\ 0 \end{bmatrix}, & x \le 0, \\ \begin{bmatrix} \tau_R & 1 \\ -\delta_R & 0 \end{bmatrix} \begin{bmatrix} x \\ y \end{bmatrix} + \begin{bmatrix} 1 \\ 0 \end{bmatrix}, & x \ge 0. \end{cases}$$

- Here $(x,y) \in \mathbb{R}^2$, and $\xi = (\tau_L, \delta_L, \tau_R, \delta_R) \in \mathbb{R}^4$ are the parameters.

Phase portrait of a chaotic attractor

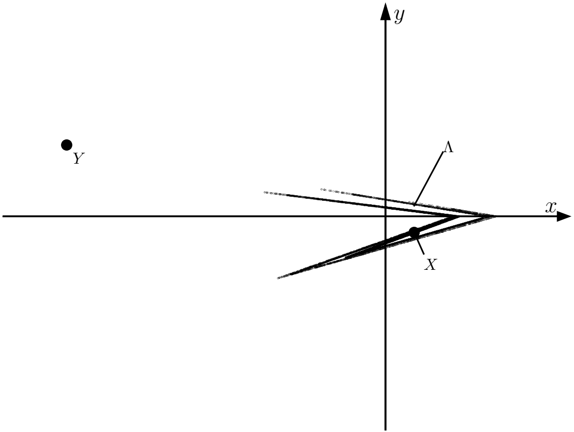

Figure: A sketch of the phase portrait of f_ξ with $\xi \in \Phi_{\mathrm{BYG}}$.

Renormalisation operator I

- Renormalisation involves showing that, for some member of a family of maps, a higher iterate or induced map is conjugate to different member of this family of maps.
- Although the second iterate f_ξ^2 has four pieces, relevant dynamics arise in only two of these. We have

$$f_\xi^2(x,y) = \begin{cases} \begin{bmatrix} \tau_L\tau_R - \delta_L & \tau_R \\ -\delta_R\tau_L & -\delta_R \end{bmatrix} \begin{bmatrix} x \\ y \end{bmatrix} + \begin{bmatrix} \tau_R + 1 \\ -\delta_R \end{bmatrix}, & x \le 0, \\ \begin{bmatrix} \tau_R^2 - \delta_R & \tau_R \\ -\delta_R\tau_R & -\delta_R \end{bmatrix} \begin{bmatrix} x \\ y \end{bmatrix} + \begin{bmatrix} \tau_R + 1 \\ -\delta_R \end{bmatrix}, & x \ge 0. \end{cases}$$

- Now f_ξ^2 can be transformed to $f_{g(\xi)}$, where g is the *renormalisation operator* (Ghosh & Simpson, 2022.) $g : \mathbb{R}^4 \to \mathbb{R}^4$, given by

$$\begin{aligned}
\tilde{\tau}_L &= \tau_R^2 - 2\delta_R, \\
\tilde{\delta}_L &= \delta_R^2, \\
\tilde{\tau}_R &= \tau_L\tau_R - \delta_L - \delta_R, \\
\tilde{\delta}_R &= \delta_L\delta_R.
\end{aligned}$$

- We perform a coordinate change to put f_ξ^2 in the normal form :

$$\begin{bmatrix} \tilde{x}' \\ \tilde{y}' \end{bmatrix} = \begin{cases} \begin{bmatrix} \tilde{\tau}_L & 1 \\ -\tilde{\delta}_L & 0 \end{bmatrix} \begin{bmatrix} \tilde{x} \\ \tilde{y} \end{bmatrix} + \begin{bmatrix} 1 \\ 0 \end{bmatrix}, & \tilde{x} \le 0, \\ \begin{bmatrix} \tilde{\tau}_R & 1 \\ -\tilde{\delta}_R & 0 \end{bmatrix} \begin{bmatrix} \tilde{x} \\ \tilde{y} \end{bmatrix} + \begin{bmatrix} 1 \\ 0 \end{bmatrix}, & \tilde{x} \ge 0. \end{cases}$$

Results I

- We consider the parameter region

$$\Phi = \left\{ \xi \in \mathbb{R}^4 \middle| \tau_L > \delta_L + 1, \delta_L > 0, \tau_R < -(\delta_R + 1), \delta_R > 0 \right\}.$$

- The stable and the unstable manifolds of the fixed point Y intersect if and only if $\zeta_0(\xi) \leq 0$.
- The attractor is often destroyed at $\zeta_0(\xi) = 0$ which is a homoclinic bifurcation (Banerjee, Yorke & Grebogi, 1998), and thus focused their attention on the region

$$\Phi_{\mathrm{BYG}} = \{ \xi \in \Phi | \zeta_0(\xi) > 0 \}.$$

Results II

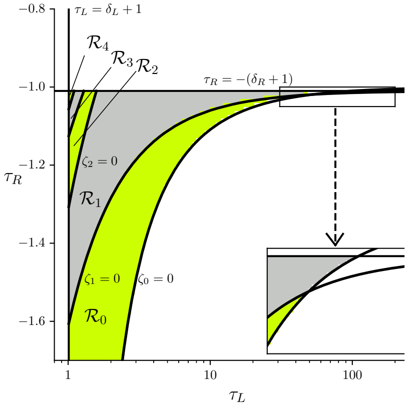

Figure: The sketch of two-dimensional cross-section of Φ_{BYG} when $\delta_L = \delta_R = 0.01$.

Results III

Theorem (Ghosh & Simpson, 2022)

The $\mathcal{R}_n$ are non-empty, mutually disjoint, and converge to the fixed point $(1, 0, -1, 0)$ as $n \to \infty$. Moreover,

$$\Phi_{\mathrm{BYG}} \subset \bigcup_{n=0}^{\infty} \mathcal{R}_n.$$

- Let,

$$\Lambda(\xi) = \mathrm{cl}(W^u(X)).$$

Theorem (Ghosh & Simpson, 2022)

For the map f_ξ with any $\xi \in \mathcal{R}_0$, $\Lambda(\xi)$ is bounded, connected, and invariant. Moreover, $\Lambda(\xi)$ is chaotic (positive Lyapunov exponent).

Results IV

Theorem (Ghosh & Simpson, 2022)

For any $\xi \in \mathcal{R}_n$ where $n \geq 0$, $g^n(\xi) \in \mathcal{R}_0$ and there exist mutually disjoint sets $S_0, S_1, \ldots, S_{2^n-1} \subset \mathbb{R}^2$ such that $f_\xi(S_i) = S_{(i+1) \text{ mod } 2^n}$ and

$$f_\xi^{2^n}|_{S_i} \text{ is affinely conjugate to } f_{g^n(\xi)}|_{\Lambda(g^n(\xi))}$$

for each $i \in \{0, 1, \ldots, 2^n - 1\}$. Moreover,

$$\bigcup_{i=0}^{2^n-1} S_i = \mathrm{cl}(W^u(\gamma_n)),$$

where γ_n is a saddle-type periodic solution of our map f_ξ having the symbolic itinerary $\mathcal{F}^n(R)$ given by Table 1.

n	$\mathcal{F}^n(\mathcal{W})$
0	R
1	LR
2	$RRLR$
3	$LRLRRRLR$
4	$RRLRRRLRLRLRRRLR$

Table: The first 5 words in the sequence generated by repeatedly applying the substitution rule $(L, R) \mapsto (RR, LR)$ to $\mathcal{W} = R$.

Results VI

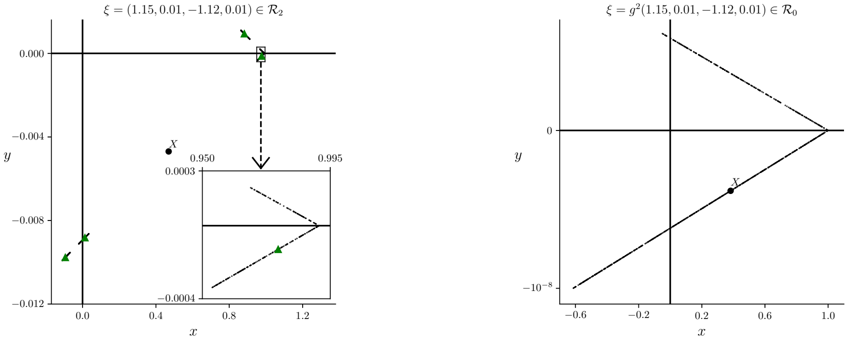

$\xi = (1.15, 0.01, -1.12, 0.01) \in \mathcal{R}_2$
0.000
−0.004
−0.008
−0.012
0.0
0.4
0.8
1.2
x
y
X
0.950
0.995
0.0003
−0.0004
$\xi = g^2(1.15, 0.01, -1.12, 0.01) \in \mathcal{R}_0$
0
-10^{-8}
−0.6
−0.2
0.2
0.6
1.0
x
y
X

Now we consider the more generalised parameter region considering the orientation-reversing and non-invertible cases,

$$\Phi = \left\{ \xi \in \mathbb{R}^4 \,|\, \tau_L > |\delta_L + 1|,\, \tau_R < |\delta_R + 1| \right\},$$

where we define

$$\Phi_{\rm trap} = \{\xi \in \Phi |\ \phi_i(\xi) > 0, i = 1, \ldots, 5\},$$

and

$$\Phi_{\rm cone} = \{\xi \in \Phi | \theta_i(\xi) \geq 0, i = 1, \ldots, 3\}.$$

Typical phase portraits I

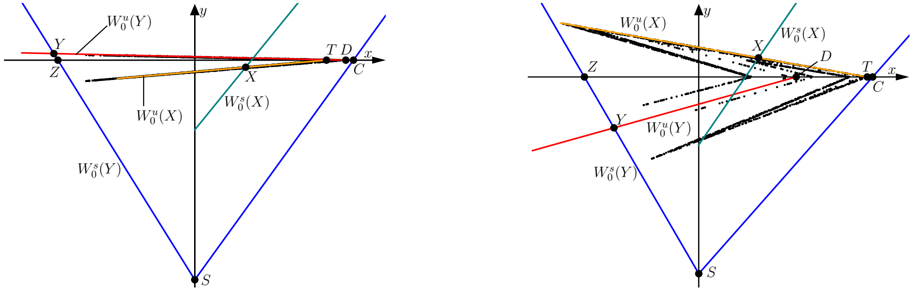

(a) $\delta_L > 0, \delta_R > 0$

(b) $\delta_L < 0, \delta_R < 0$

Figure: Typical phase portraits of the chaotic attractor for the invertible case ($\delta_L \delta_R > 0$).

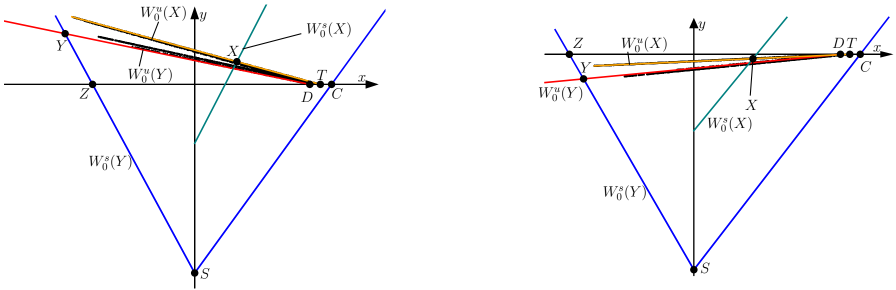

(a) $\delta_L > 0, \delta_R < 0$

(b) $\delta_L < 0, \delta_R > 0$

Figure: Typical phase portraits of the chaotic attractor for the non-invertible case ($\delta_L \delta_R < 0$).

Chaos in Φ_{BYG} can be proved by constructing an invariant expanding cone in tangent space (Glendinning & Simpson, 2021). We have extended this to Φ.

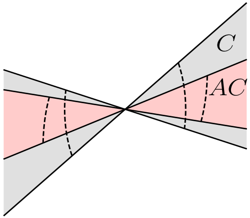

Figure: A sketch of an invariant expanding cone C and its image $AC = \{Av | v \in C\}$, given $A \in \mathbb{R}^{2\times 2}$.

Results I

Theorem (Ghosh, McLachlan, & Simpson, 2023)

For any $\xi \in \Phi_{\mathrm{trap}} \cap \Phi_{\mathrm{cone}}$, the normal form f_ξ has a topological attractor with a positive Lyapunov exponent.

- Our construction of a trapping region requires

$$
\begin{aligned}
\phi_1(\xi) &= \delta_R - \tau_R \lambda_L^u, \\
\phi_2(\xi) &= \delta_R(\lambda_L^s + 1) - \lambda_L^u(\tau_R + (\delta_R + \tau_R)\lambda_L^s), \\
\phi_3(\xi) &= \delta_R - (\delta_R + \tau_R - (\tau_R + 1)\lambda_L^u)\lambda_L^u, \\
\phi_4(\xi) &= \delta_R - (\tau_R + \delta_L + \delta_R - (1 + \tau_R)\lambda_L^u)\lambda_L^u, \\
\phi_5(\xi) &= \delta_R - (\delta_R + \tau_R - (1 + \lambda_R^u)\lambda_L^u)\lambda_L^u.
\end{aligned}
$$

- The construction of an invariant expanding cone requires

$$\theta_1(\xi) = (\delta_L + \delta_R - \tau_L \tau_R)^2 - 4\delta_L \delta_R \,, \tag{1}$$

$$\theta_2(\xi) = \tau_L^2 + \delta_L^2 - 1 + 2\tau_L \min\left(0, -\frac{\delta_R}{\tau_R}, q_L, \tilde{a}\right) \,, \tag{2}$$

$$\theta_3(\xi) = \tau_R^2 + \delta_R^2 - 1 + 2\tau_R \max\left(0, -\frac{\delta_L}{\tau_L}, q_R, \tilde{b}\right) \,, \tag{3}$$

where

$$q_L = -\frac{\tau_L}{2}\left(1 - \sqrt{1 - \frac{4\delta_L}{\tau_L^2}}\right), \qquad q_R = -\frac{\tau_R}{2}\left(1 - \sqrt{1 - \frac{4\delta_R}{\tau_R^2}}\right),$$

Results III

and

$$\tilde{a} = \frac{\delta_L - \delta_R - \tau_L \tau_R - \sqrt{\theta_1(\xi)}}{2\tau_R}, \qquad \tilde{b} = \frac{\delta_R - \delta_L - \tau_L \tau_R - \sqrt{\theta_1(\xi)}}{2\tau_L},$$

assuming $\theta_1(\xi) > 0$.

Results IV

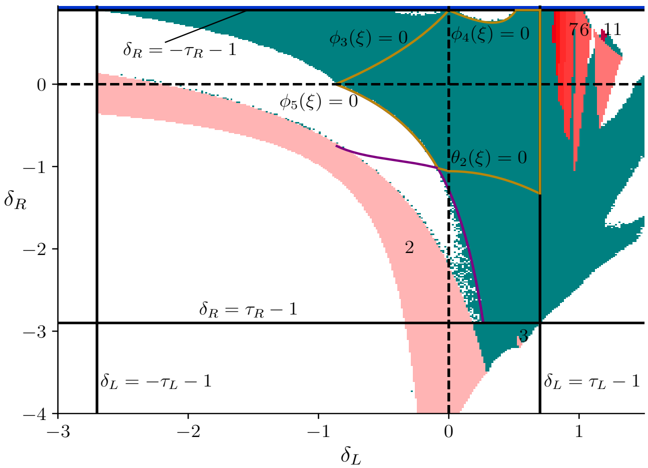

Figure: A 2D slice of $\Phi_{\mathrm{trap}} \cap \Phi_{\mathrm{cone}} \subset \mathbb{R}^4$.

Require: $k > 0, P > 0$
Ensure: $\xi \in \Phi^{(1)} \cup \Phi^{(2)} \cup \Phi^{(3)} \cup \Phi^{(4)}$ ▷ $\Phi^{(1)} = \Phi_{\mathrm{BYG}}$

$s = 1$;

Q = set of the last P points of Λ evaluated for the parameter set ξ ;

C = complete graph of the nodelist Q with edges between the node points having weights according to the distance formula

$$\sqrt{(\Delta x)^2 + \left(\frac{\Delta y}{\max(\delta_L, \delta_R)}\right)^2};$$

E = weights from $\mathrm{MinimumSpanningTree}(C)$; ▷ (Robins, Meiss & Bradley, 2000)

$d = k \times \mathrm{median}(E)$;

while an edge in E has weight greater than d **do**

  $s = s + 1$;

end while

- Let

$$\Phi^{(2)} = \{\xi \in \Phi \mid \delta_L < 0, \delta_R < 0, \alpha(\xi) < 0, \theta(\xi) > 0\},$$

where

$$\alpha(\xi) = \tau_L \tau_R + \delta_L \delta_R - (\delta_L + \delta_R) + 1.$$

For $n \geq 1$, the n^{th} preimage of the surface $\theta(\xi) = 0$ under g is given by

$$\zeta_n^{(2)}(\xi) = \zeta_{n-1}^{(1)}(g(\xi)) = \phi(g^n(\xi)),$$

with

$$\zeta_0^{(2)}(\xi) = \theta(\xi).$$

Extension of Renormalisation to other quadrants II

Proposition (Ghosh, McLachlan, & Simpson, 2023)

If $\xi \in \Phi^{(2)}$, then $g(\xi) \in \Phi^{(1)}$.

Note that g is well-defined with

$$g^{-1}(\xi) = \left(-\frac{\tau_R - \frac{\delta_R}{\sqrt{\delta_L}} - \sqrt{\delta_L}}{\sqrt{\tau_L - 2\sqrt{\delta_L}}}, -\frac{\delta_R}{\sqrt{\delta_L}}, -\sqrt{\tau_L - 2\sqrt{\delta_L}}, -\sqrt{\delta_L} \right).$$

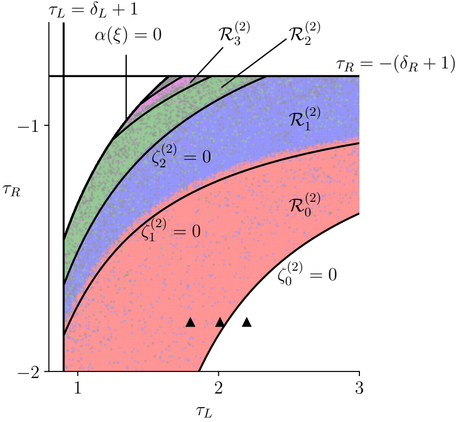

Figure: The sketch of two-dimensional cross-section of $\Phi^{(2)}$, when $\delta_L = -0.1$ and $\delta_R = -0.2$.

Extension of Renormalisation to other quadrants IV

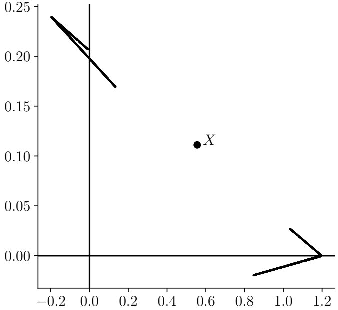

(a) $\xi = \xi_{\mathrm{ex}}^{(2)} \in \mathcal{R}_1^{(2)}$

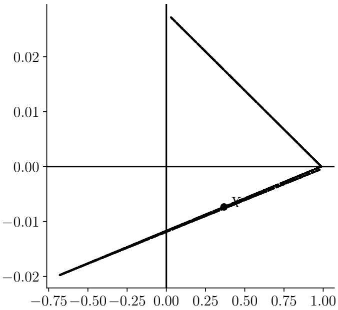

(b) $\xi = g(\xi_{\mathrm{ex}}^{(2)}) \in \mathcal{R}_0^{(1)}$

Extension of Renormalisation to other quadrants V

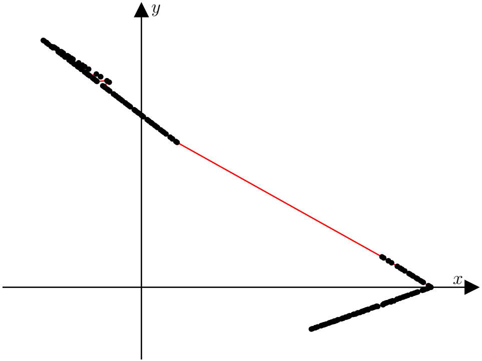

Figure: Minimum spanning tree for $P = 200$ data points of Λ for $\xi \in \Phi^{(2)}$, with $k = 10$.

Extension of Renormalisation to other quadrants VI

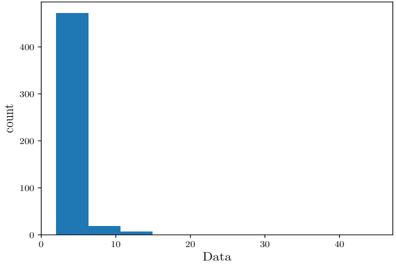

Figure: Histogram of the number of components of the attractor for $\xi = (1.4, -0.1, -1.2, -0.2)$. Notice that the number 2 appears 73.4% of the times, indicating our algorithm having a good performance rate.

- Let

$$\Phi^{(3)} = \{\xi \in \Phi \mid \delta_L > 0, \delta_R < 0, \alpha(\xi) < 0, \min(\phi(\xi), \theta(\xi)) > 0\},$$

meaning the map is invertible. After close inspection, it is observed that the attractor gets destroyed partly at the homoclinic corner $\phi(\xi) = 0$ and partly at the heteroclinic corner $\theta(\xi) = 0$. This lets us define the surface $\zeta_0^{(3)}(\xi)$ as

$$\zeta_0^{(3)}(\xi) = \min(\phi(\xi), \theta(\xi)).$$

For $n \geq 0$, the n^{th} preimage of the surface $\zeta_0^{(3)}(\xi) = 0$ under g is represented by

$$\zeta_n^{(3)}(\xi) = \min(\phi(g^n(\xi)), \theta(g^n(\xi))).$$

Proposition (Ghosh, McLachlan, & Simpson, 2023)

If $\xi \in \Phi^{(3)}$, then $g(\xi) \in \Phi^{(3)}$.

Note that g is well-defined with

$$g^{-1}(\xi) = \left(-\frac{\tau_R - \frac{\delta_R}{\sqrt{\delta_L}} - \sqrt{\delta_L}}{\sqrt{\tau_L - 2\sqrt{\delta_L}}}, -\frac{\delta_R}{\sqrt{\delta_L}}, -\sqrt{\tau_L - 2\sqrt{\delta_L}}, -\sqrt{\delta_L} \right).$$

Extension of Renormalisation to other quadrants IX

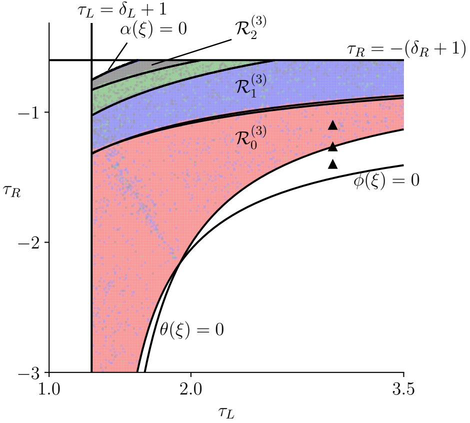

Figure: The sketch of two-dimensional cross-section of $\Phi^{(3)}$, when $\delta_L = 0.3$ and $\delta_R = -0.4$.

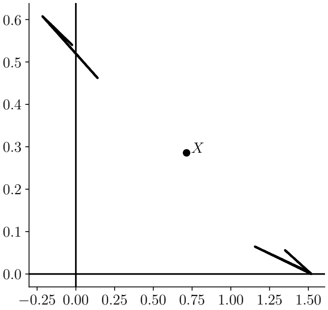

(a) $\xi = \xi_{\text{ex}}^{(3)} \in \mathcal{R}_1^{(3)}$

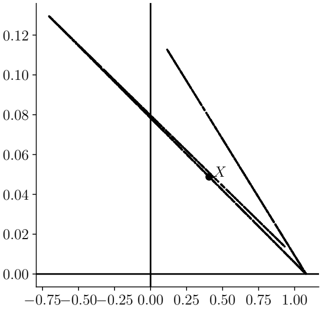

(b) $\xi = g(\xi_{\text{ex}}^{(3)}) \in \mathcal{R}_0^{(3)}$

Extension of Renormalisation to other quadrants XI

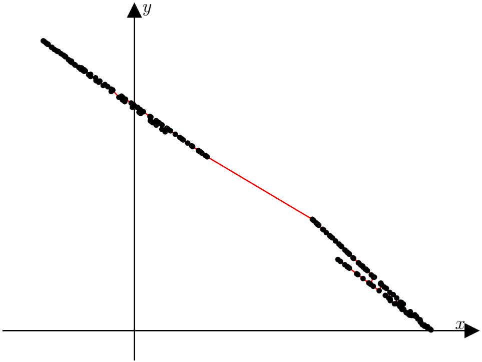

Figure: Minimum spanning tree for $P = 200$ data points of Λ for $\xi \in \Phi^{(3)}$, with $k = 10$.

- let

$$\Phi^{(4)} = \{\xi \in \Phi \mid \delta_L < 0, \delta_R > 0, \alpha(\xi) < 0, \theta(\xi) > 0\},$$

representing the other quadrant where the map is non-invertible.

Proposition (Ghosh, McLachlan, & Simpson, 2023.)

If $\xi \in \Phi^{(4)}$, then $g(\xi) \in \Phi^{(3)}$.

Note that g is well-defined with

$$g^{-1}(\xi) = \left(-\frac{\tau_R - \frac{\delta_R}{\sqrt{\delta_L}} - \sqrt{\delta_L}}{\sqrt{\tau_L - 2\sqrt{\delta_L}}}, -\frac{\delta_R}{\sqrt{\delta_L}}, -\sqrt{\tau_L - 2\sqrt{\delta_L}}, -\sqrt{\delta_L}\right).$$

Note that g is again well-defined with

$$g^{-1}(\xi) = \left(-\frac{\tau_R + \frac{\delta_R}{\sqrt{\delta_L}} + \sqrt{\delta_L}}{\sqrt{\tau_L + 2\sqrt{\delta_L}}}, \frac{\delta_R}{\sqrt{\delta_L}}, -\sqrt{\tau_L + 2\sqrt{\delta_L}}, \sqrt{\delta_L} \right).$$

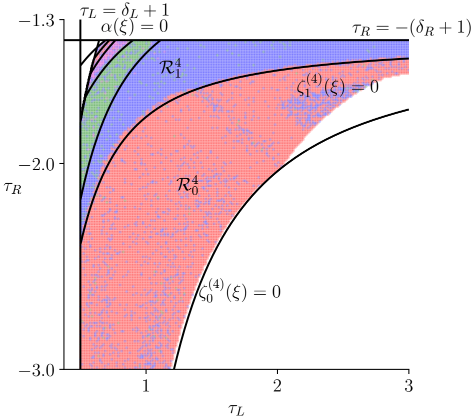

Figure: The sketch of two-dimensional cross-section of $\Phi^{(3)}$, when $\delta_L = -0.5$ and $\delta_R = 0.4$.

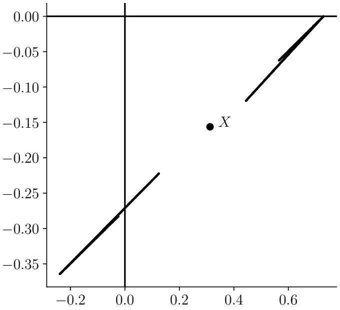

(a) $\xi = \xi_{\mathrm{ex}}^{(4)} \in \mathcal{R}_1^{(4)}$

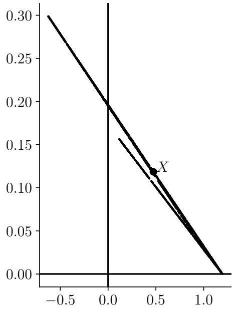

(b) $\xi = g(\xi_{\mathrm{ex}}^{(4)}) \in \mathcal{R}_0^{(3)}$

Extension of Renormalisation to other quadrants XVI

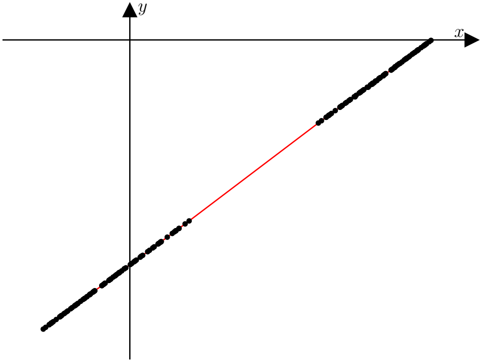

Figure: Minimum spanning tree for $P = 200$ data points of Λ for $\xi \in \Phi^{(4)}$, with $k = 10$.

Summary

- We have used renormalisation to explain how the parameter space Φ_{BYG} is divided into regions according to the number of connected components of an attractor.
- We have further shown how the robust chaos extends more broadly to orientation-reversing and non-invertible piecewise-linear maps.
- We have also extended the application of renormalisation to the orientation-reversing and non-invertible map in a more generalised parameter setting.
- It remains to determine the analogue of the existence of a higher dimensional robust chaos parameter region of the border-collision normal form.

Acknowledgements

Our research is supported by Marsden Fund contract MAU1809, managed by the Royal Society Te Apārangi.

Thank you! Questions?